

A comparison between soft x-ray and magnetic phase data on the Madison symmetric torus

P. D. VanMeter, P. Franz, L. M. Reusch, J. S. Sarff, and D. J. Den Hartog

Citation: *Rev. Sci. Instrum.* **87**, 11E322 (2016); doi: 10.1063/1.4960492

View online: <http://dx.doi.org/10.1063/1.4960492>

View Table of Contents: <http://aip.scitation.org/toc/rsi/87/11>

Published by the [American Institute of Physics](#)



SHIMADZU
Excellence in Science

**Powerful, Multi-functional UV-Vis-NIR and
FTIR Spectrophotometers**

Providing the utmost in sensitivity, accuracy and resolution for applications in materials characterization and science

- Photovoltaics
- Polymers
- Coatings
- Paints
- Ceramics
- Thin films
- Inks
- DNA film structures
- Packaging materials
- Nanotechnology

[Click here for accurate, cost-effective laboratory solutions](#)



A comparison between soft x-ray and magnetic phase data on the Madison symmetric torus

P. D. VanMeter,^{1,a)} P. Franz,² L. M. Reusch,¹ J. S. Sarff,¹ and D. J. Den Hartog¹

¹University of Wisconsin-Madison, Madison, Wisconsin 53706, USA

²Consorzio RFX, Padova, Italy

(Presented 8 June 2016; received 5 June 2016; accepted 15 July 2016; published online 15 August 2016)

The Soft X-Ray (SXR) tomography system on the Madison Symmetric Torus uses four cameras to determine the emissivity structure of the plasma. This structure should directly correspond to the structure of the magnetic field; however, there is an apparent phase difference between the emissivity reconstructions and magnetic field reconstructions when using a cylindrical approximation. The difference between the phase of the dominant rotating helical mode of the magnetic field and the motion of the brightest line of sight for each SXR camera is dependent on both the camera viewing angle and the plasma conditions. Holding these parameters fixed, this phase difference is shown to be consistent over multiple measurements when only toroidal or poloidal magnetic field components are considered. These differences emerge from physical effects of the toroidal geometry which are not captured in the cylindrical approximation. *Published by AIP Publishing.* [<http://dx.doi.org/10.1063/1.4960492>]

I. INTRODUCTION

The Soft X-Ray (SXR) diagnostic system was constructed on the Madison Symmetric Torus (MST)¹ in order to aid in the study of resistive tearing modes via tomographic reconstruction of emissivity.² The current system consists of four cameras spaced at different poloidal angles around a single toroidal position, labeled by the letters A-D, with each of these consisting of ten individual viewing chords. Each chord measures the brightness of the plasma, which is the line-integral of the plasma emissivity,³ using two Be filters of different thickness. A cross-sectional map of the emissivity of the plasma can then be reconstructed through a variety of techniques,⁴ or the electron temperature can be directly computed from the ratio of the brightness data between the thick and thin sets of foils.^{3,5}

It has been previously established that there is a direct correspondence between magnetic island structures and SXR emissivity structures.⁶ These structures appear during quasi-single helicity (QSH) states,⁷ where a single $m = 1$ tearing mode dominates the magnetic spectrum. This paper grew out of an attempt to further characterize this relation at MST. Instead of performing a full tomographic inversion, this technique examines the oscillating raw brightness of the plasma during a QSH state and shows that this corresponds directly to the oscillation of the dominant magnetic mode in a cylindrical approximation, up to a phase shift.

The value of this phase shift, however, is found to be dependent on the plasma conditions and whether the structure is compared to the poloidal or toroidal component of the magnetic field. These deviations are consistent with the effects of toroidal mode-mixing and make the case that consideration

of these effects is essential when comparing measurements between diagnostics located at different toroidal and poloidal angles.

II. ESTIMATING THE PHASE OF THE SXR EMISSIVITY STRUCTURE

In order to explore the relation between the phase of the dominant mode of the magnetic field and the rotation of the soft x-ray emissivity structure, it is important to first characterize these structures in a self-consistent way. The magnetics array on MST¹ measures the amplitudes of both the toroidal and poloidal components of the magnetic field at the device wall, at poloidal angle $\theta_{mag} = 241^\circ$, where $\theta = 0$ is the outboard mid-plane. At every time step, these amplitudes are independently fit to a Fourier spectrum of the form

$$B(\phi) = \sum_{n=-\infty}^{\infty} c_n \cos(n\phi - \delta_n). \quad (1)$$

Here $B(\phi)$ may be either the poloidal or toroidal component of the magnetic field, and δ_n is the phase of the n th mode. Since the one-dimensional magnetic array is at a fixed poloidal angle, it does not resolve poloidal harmonics, denoted by the mode number m . In practice, however, this is not a problem since the $m = 1$ mode tends to dominate core tearing mode instabilities in MST.⁸

This analysis considers only periods of time in which the magnetic field decomposition is dominated by a single mode number, n , and in which the mode is not wall-locked. This can sometimes happen via an electromagnetic braking torque associated with eddy current in the metal shell surrounding the plasma. Under these conditions, the poloidal position of the magnetic O-point at a given toroidal location ϕ is given by

$$\theta_{op,n}(t) = n\phi + \theta - \delta_n(t). \quad (2)$$

Note: Contributed paper, published as part of the Proceedings of the 21st Topical Conference on High-Temperature Plasma Diagnostics, Madison, Wisconsin, USA, June 2016.

^{a)}Electronic mail: pvanmeter@wisc.edu

This relation assumes cylindrical symmetry, which is often sufficient for describing RFP dynamics. The consequence of the actual toroidal geometry is one of the main points of this paper and the topic of discussion in Section IV.

The soft X-ray diagnostic on MST consists of four individual x-ray cameras, each at the same toroidal angle ($\phi = 90^\circ$) and different poloidal angles. Although the system is capable of performing a full tomographic reconstruction to produce an emissivity map of a cross section of the plasma, for this analysis, it suffices to consider only the raw brightness data. If it is assumed that the brightest point in the plasma corresponds to the O-point of the rotating magnetic island structure,⁷ then the impact parameter of the brightest line of sight for a given SXR camera can be expected to oscillate like

$$p_{max}^S(t) = A_0^S - (A_1^S)^2 \sin(\theta_{op}(t) - \theta^S + F(f)), \quad (3)$$

where $S \in \{A, B, C, D\}$ is the SXR camera label. The impact parameter p is the distance of the line of sight from the geometric axis. A_0 and A_1 are fitting parameters determining the offset and amplitude of the oscillation. These vary by camera location and are not important to the analysis presented here. θ^S is the poloidal angle of the camera S . $F(f)$ is an additional function to account for the frequency-dependence of the digital amplifiers. In this analysis, $F(f)$ is assumed to behave approximately as a first-order polynomial determined from a prior calibration of the equipment.

Making the assumptions that lead to Equation (2), the argument of the sinusoidal term can be rewritten in terms of another fitting parameter and the phase of the dominant magnetic mode,

$$\begin{aligned} \theta_{op}(t) - \theta^S &= (n \times 90^\circ + 241^\circ - \theta^S - \Delta\delta) - \delta_n(t) \\ &\equiv A_2^S - \delta_n(t). \end{aligned} \quad (4)$$

An additional term, $\Delta\delta$, is introduced here as a measure of the deviation from cylindrical geometry to account for effects related to toridicity. That is, if the cylindrical approximation is a good assumption, then it will be found that $\Delta\delta = 0$. This is the parameter that this paper is concerned with measuring.

In order to determine the maximum impact parameter for a given camera at a given instant in time, it is necessary to interpolate between the ten available lines of sight. This is done most easily by fitting a second-order polynomial in the impact parameter to the raw brightness data via a standard SVD-fit routine⁹ and determining the coordinate which maximizes that function. An example of this type of fit, as well as the quality of the quadratic approximation, is shown in Fig. 1.

This technique can be performed over multiple timesteps in order to produce the time evolution of p_{max}^S for each of the four cameras. These data are then fitted to the functional form of Equation (3) with the argument of the sinusoidal term written in the form of Equation (4). This was performed via a nonlinear least-squares algorithm,⁹ using $\Delta\delta = 0$ as the starting point for the computation and taking the values of $\delta_n(t)$ directly from the magnetic array measurements. Fig. 2 shows data points from a typical QSH period as observed for camera A and its best fit. The fit is qualitatively good, with some deviation expected due to the minimal presence of other

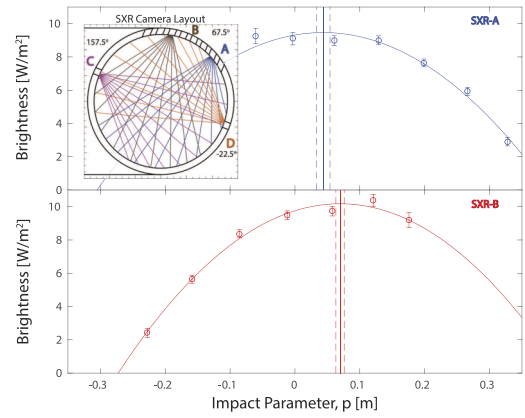


FIG. 1. Example of the SXR brightness data vs. impact parameter fit to a quadratic polynomial for cameras A (top) and B (bottom). The lines show the location of peak brightness and associated uncertainty. The SXR camera layout is also shown.

toroidal modes. We also observe good agreement between the frequency of the SXR and magnetics array datasets.

The data obtained through this method can be compared against data synthetically generated using a perfect cylindrical geometry. This was performed with a computer simulation of the SXR system, assuming a 6 cm Shafranov shift and a single hot island ($T_{e,max} = 1350$ eV for the bulk and 1650 eV for the island). This helical structure was considered at several different poloidal angles, and the simulated magnetic phase was calculated using Equation (4) with $\Delta\delta = 0$, thus assuming exactly one dominant toroidal mode and perfect cylindrical geometry. This provides a value of the fit parameter A_2^S which takes into account the effects of diagnostic geometry. $\Delta\delta$ is then determined by comparing the value of A_2^S as determined from the data to this “ideal case.”

III. SUMMARY OF RESULTS

Using the procedures described in Section II, the parameter $\Delta\delta$ was calculated for four different cases, considering two different sets of plasma conditions and considering the phase of both the poloidal and toroidal magnetic field components separately. The two different sets of plasma conditions considered, referred to as Pulsed Poloidal Current Drive (PPCD)^{10,11}

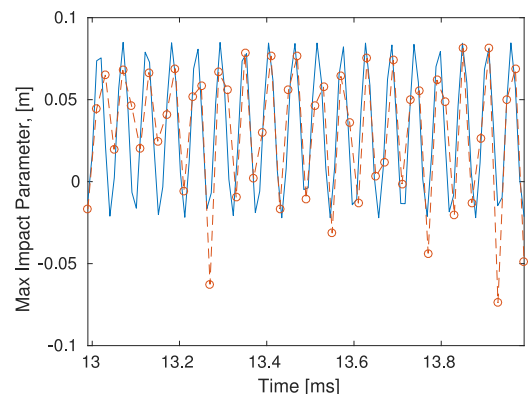


FIG. 2. Oscillation of the impact parameter of the brightest line of sight over time for shot # 1150324080. The points represent data, and the solid line is the fit model.

TABLE I. Average $\Delta\delta$ comparison (PPCD, $n = 6$).

	SXR-A	SXR-B	SXR-C	SXR-D	Average
Mean $\Delta\delta_\theta$	1.32	-9.32	-2.50	3.01	-1.87
St. dev.	8.85	10.63	11.90	9.44	
Mean $\Delta\delta_\phi$	-26.11	-36.86	-30.52	-25.86	-29.84
St. dev.	8.85	10.78	11.45	9.41	

TABLE II. Average $\Delta\delta$ comparison (QSH, $n = 5$).

	SXR-A	SXR-B	SXR-C	SXR-D	Average
Mean $\Delta\delta_\theta$	-16.13	-21.60	-13.59	-14.12	-16.36
St. dev.	8.05	7.92	12.12	8.26	
Mean $\Delta\delta_\phi$	-46.17	-49.67	-42.94	-44.03	-45.70
St. dev.	8.80	8.48	12.37	8.65	

and QSH, produce quasi-single helicity states that are dominated by different toroidal modes ($n = 6$ for PPCD, $n = 5$ for QSH). The magnetic phases considered, $\delta_{n,\theta}$ and $\delta_{n,\phi}$, were taken from the poloidal and toroidal magnetic field decompositions, respectively. The cylindrical model predicts these phases to differ by 180° .

The results of this analysis are given in Tables I and II, taken from a sample size of about 40 shots/case. In both PPCD and QSH plasmas, $\Delta\delta$ is nonzero. The mean value of $\Delta\delta$ varies between cameras for a given set of conditions. Measurements from SXR-B are always seen to have a more negative value of $\Delta\delta$ than the other cameras, regardless of conditions. This is likely an effect of the camera viewing angle and suggests a poloidal dependence. It is also notable that in both plasma conditions, the difference between $\Delta\delta_\phi$ and $\Delta\delta_\theta$ is about 29° , which differs substantially from the cylindrical model.

There is a noticeable shift between the PPCD and QSH cases of about 15° on average, although this effect too displays a consistent dependence on viewing angle. This observation suggests a dependence on the dominant mode number, which relates to the radial location of the relevant rational surface.

IV. THE IMPORTANCE OF TOROIDAL EFFECTS TO SXR MEASUREMENTS

The deviations from the cylindrical model discussed above are due at least in part to the influence of toroidal

effects, which the model ignores. Such a geometry can lead to a mixing effect between poloidal modes,¹² which in turn can cause significant shifts in the expected phase of observed instabilities. Work is currently underway to compare these measurements to simulations of core tearing modes in a toroidal geometry using the NIMROD code,¹³ and preliminary results display features consistent with these observations.

Future work will focus on quantifying any remaining systematic effects on the phase due to finite bandwidth of the distinct electronics and digitizer timing and on making more quantitative comparisons to computer simulations of plasmas in a toroidal geometry. However, the analysis presented here is sufficient to emphasize the importance of taking toroidal effects into consideration when comparing measurements from the SXR tomography system with measurements taken from diagnostics at other toroidal positions. Failing to account for these effects could lead to a misinterpretation of measurements.

ACKNOWLEDGMENTS

This material is based upon work supported by the U.S. Department of Energy Office of Science, Office of Fusion Energy Sciences program under Award No. DE-FC02-05ER54814.

- ¹R. N. Dexter, D. W. Kerst, T. W. Lovell, S. C. Prager, and J. C. Sprott, *Fusion Technol.* **19**, 131 (1991).
- ²P. Franz, L. Marrelli, P. Piovesan, I. Predebon, F. Bonomo *et al.*, *Phys. Plasmas* **13**, 1 (2006).
- ³M. B. McGarry, P. Franz, D. J. Den Hartog, and J. A. Goetz, *Rev. Sci. Instrum.* **81**, 8 (2010).
- ⁴P. Franz, L. Marrelli, A. Murari, G. Spizzo, and P. Martin, *Nucl. Fusion* **41**, 695 (2001).
- ⁵F. C. Jahoda, E. M. Little, W. E. Quinn, G. A. Sawyer, and T. F. Stratton, *Phys. Rev.* **119**, 843 (1960).
- ⁶D. F. Escande, P. Martin, S. Ortolani, A. Buffa, P. Franz *et al.*, *Phys. Rev. Lett.* **85**, 1662 (2000).
- ⁷P. Franz, M. Gobbin, L. Marrelli, A. Ruzzon, A. Fassina, E. Martines, and G. Spizzo, *Nucl. Fusion* **53**, 053011 (2013).
- ⁸S. Choi, Ph.D. thesis, University of Wisconsin-Madison, 2006.
- ⁹W. H. Press, B. P. Flannery, S. A. Teukolsky, and W. T. Vetterling, *Numerical Recipes in C* (Cambridge University Press, 1993).
- ¹⁰J. Sarff, S. Hokin, H. Ji, S. Prager, and C. Sovinec, *Phys. Rev. Lett.* **72**, 3670 (1994).
- ¹¹M. Puiatti, S. Cappello, R. Lorenzini, S. Martini, S. Ortolani *et al.*, *Nucl. Fusion* **43**, 1057 (2003).
- ¹²P. Zanca and D. Terranova, *Plasma Phys. Controlled Fusion* **46**, 1115 (2004).
- ¹³C. R. Sovinec, A. H. Glasser, T. A. Gianakon, D. C. Barnes, R. A. Nebel *et al.*, *J. Comput. Phys.* **195**, 355 (2004).